Measurement of wall shear stress on flow over a wall change from rough to smooth

Fernanda B. C. C. Sousa
Atila P. Silva Freire
Mechanical Engineering Program (COPPE/UFRJ), C.P. 68503, 21945-970, Rio de Janeiro, Brazil

José L. Z. Zotin
Juliana B. R. Loureiro
Scientific Division, Inmetro, 22.050-050, Rio de Janeiro, Brazil

Abstract. *The present work uses laser Doppler anemometry and particle image velocimetry to characterize the transitional flow in regions where abrupt changes in surface momentum flux occur due to changes from one extensive uniform rough surface to another extensive uniform smooth surface. The work analyzes the statistics of the flow to show that none of the classical methods for the evaluation of the wall shear stress can be used in a rough-to-smooth transition region. The concept of zero-plane displacement is also investigated in detail in connection with the theoretical estimation of the wall shear stress.*

Keywords: *roughness, skin-friction, zero-plane displacement.*

1. INTRODUCTION

The wall shear stress is a parameter of particular practical and theoretical interest. The asymptotic structure of the canonical boundary layer, for example, is constructed on the basis of a reference velocity defined in terms of the wall shear stress. Turbulence models and calculation methods are also strongly dependent on the wall shear stress (τ_w) for a definition of their relevant scales and wall boundary conditions.

For flows in equilibrium conditions, various procedures have been developed to estimate τ_w. Even so, the difficulties are many. Indeed, in the classical methods, including the velocity gradient method, the Preston tube and the constant shear stress hypothesis of Prandtl, much caution must be exercised in their application.

In problems where surface roughness change, a flowing fluid does not immediately adapt at all heights to the local wall conditions, but does so in a layer adjacent to the wall normally referred to as the internal boundary layer (IBL) (Blom and Wartena, 1969). Above this layer, the flow is characteristic of the upstream conditions except for changes resulting from a flow acceleration-term and a term representing the velocity change due to the displacement of the streamlines (Townsend, 1965). The development of the internal boundary layer with downstream distance was early studied by Blom and Vartena (1969), who showed that while velocity profiles evaluated from previously advanced theories (Elliot (1958), Panofsky and Townsend (1964) and Townsend (1965)) agree well with experiments, predictions for the wall shear stress disagree strongly.

A recent and important contribution to experimental study on roughness change is the work of Cheng and Castro (2002). Their particular concern was to characterize well the roughness sublayer. The common expectation is that downstream of a step change with a substantial increase in roughness, there exists a sublayer – the lowest 10% of the IBL – in which (i) a constant shear stress layer is formed in equilibrium with the new roughness and (ii) the mean velocity is caracterised by a logarithmic profile (Kaimal and Finnigan, 1993). In this region, the inertial sublayer (IS), the flow is horizontally homogeneously and similarity theories are applicable. Below the IS, there is a region – the roughness sublayer (RS) – where the geometry of the roughness strongly influences the flow properties. In this region, the existing inhomogeneities make it very difficult to interpret the flow statistics, including the wall shear stress. Cheng and Castro (2002) identify the downstream fetch needed before flow similar is achieved and a logarithmic region can be observed. The downstream distance the growing equilibrium layer required to encompass the RS and develop the IS was estimated to be $160z_{02}$ (z_{02} = downstream roughness length).

When changes occur from a rough to a smooth surface, the picture seems different. While the wall shear stress adjusts immediately to the new boundary condition, the shear stress in the fully turbulent region adjusts slowly. For this reason, wall shear stress calculations (τ_w) based on the slope of semi-logarithmic graphs should not, in principle, hold. In Antonia and Luxton (1972), the estimation of the wall shear stress is made through the Clauser chart method, Preston tubes and the momentum integral equation. They conclude that none of these methods provide acceptable results.

The present work studies the applicability of the velocity gradient method to estimate the friction velocity in flows subject to a step change from a rough to a smooth surface. The difficulties encountered by other authors to assess τ_w on the smooth wall are circumvented with the use of a MEMS based optical microsensor, the Diverging Fringe Doppler sensor, designed to measure the flow velocity gradient at 75 μm above the sensor surface. The small dimensions of this sensor make it an ideal instrument to measure τ_w in the adjustment flow region of a rough-to-smooth surface change. The

results are compared with Preston tube measurements.

Our main concern here is to characterize the wall shear stress in the downstream fetch required before the flow achieves equilibrium condition. The mean velocity and turbulence profiles are obtained through a two-channel laser Doppler anemometer (LDA) and a two-dimensional particle image velocimeter (PIV).

2. THEORY

2.1 The velocity gradient method

The gradient method developed by Clauser (1954) to determine the skin-friction relies on the existence of self-preservation, and, in particular, on the universality of the parameters appearing in the law of the wall. For a rough surface, this method has been modified by Perry and Joubert (1963) and by Perry et al. (1969) to account for the zero-plane displacement and the roughness length.

For a rough surface, it is possible to write

$$\frac{u}{u_*} = \frac{1}{\varkappa} \ln\left(\frac{z-d}{z_0}\right) \tag{1}$$

where, u_* is the friction velocity ($= \sqrt{(\tau_w/\rho)}$), $\varkappa = 0.4$, d is the distance from the bottom of the roughness elements to which the eddy diffusivity extrapolates to zero and z_0 is a parameter characteristic of the roughness, the roughness length.

As can be seen from Eq. 1, a plot of u against $\ln(z-d)$ in a region of equilibrium flow should furnish a straight line whose slope corresponds to the value of u_*. A major difficulty however arises from the fact that d is not known *a priori*. Many approximate methods have been proposed in literature to determine the position of the plane of displacement, d. Here, to search for values of u_* and z_0, global optimization algorithms are used. These algorithms attempt to find the global optimum by allowing decrease as well as increase of the objective/merit function. Usually they are computationally expensive. Four different methods were applied to Eq. (1) for solution search: nelder mead, differential evolution, simulated annealing and random search. Only when all four methods furnish consistent results, with accuracy down to the sixth decimal fraction, the search is stopped.

2.2 Preston tube

The principle of operation of a Preston tube is very simple since it relies solely on the difference between the pressure recorded by a pitot tube resting on a surface and the undisturbed static pressure. The underlying idea is that there exists a near wall region whose velocity distribution is mutual to boundary layers and pipe flows and is determined by the surface shear stress. This assumption gives us the means of determining the friction velocity (u_*) from calibration curves obtained in fully developed pipe flow.

Some early criticism regarding the soundness of the method of Preston to measure u_* was convincingly refuted by Head and Rechenberg (1962) and Patel (1965) through experiments conducted in strong favorable and adverse pressure gradients. In very detailed experiments, Patel (1966) established definitive calibration curves, valid in well defined intervals expressed in terms of $u_* d/2\nu$.

In the present data reduction, the surface Pitot tube had external and internal diameters of respectively 1.28 and 0.95 mm. The calibration, in the range $1.5 < \log(\tau_w d^2/4\rho\nu^2) < 3.5$, was used according with the empirical relation (Patel, 1965):

$$y^* = 0.8287 - 0.1381x^* + 0.1437(x^*)^2 - 0.0060(x^*)^2 \tag{2}$$

where $x^* = \log(\Delta p_p d^2/4\rho\nu^2)$ and $y^* = \log(\tau_w d^2/4\rho\nu^2)$.

2.3 Reynolds shear stress

Another way to find u_* is to use the hypothesis of Prandtl (1925) that across the wall layer the total shear stress deviates just slightly from the wall shear stress. The friction velocity can then evaluated from $u_* = \sqrt{-\overline{u'w'}}$.

Following the classical measurements of Reichardt (1939) and Klebanoff (1955), it has been a common practice in literature to consider $-\overline{u'w'} \approx 3/20\,\overline{u'^2}$ so that u_* can after all be estimates from measured profiles of $\sqrt{\overline{u'^2}}$.

2.4 Optical microsensor

The wall shear stress is a variable of utmost importance for modelling and prediction of turbulent flows. Although the demand for reliable wall shear stress data is high, there are a few state of the art methods available for the quantification of

this variable, such as impact probes, floating elements, thermal anemometry and oil film interferometry. However, most of these techniques have their own limitations and are usually restricted to flows under equilibrium conditions, where the classical boundary layer assumptions are valid.

In the present work, three different methods have been used to quantify the skin friction at the wall: i) the Preston tube described by Patel (1962), ii) the Micro-S sensor from Measurement Science Enterprise Inc. (Fourguette et al., 2001; Gharib et al., 2002) and iii) the slope of the velocity distribution in the logarithmic sublayer (Clauser, 1956).

The Micro-S system is comprised of a Micro-S sensor, a sensor driver unit that contains the laser source, and a burst processor, responsible for band-pass filtering and conditioning the raw signal that is digitized through a National Instruments board at the computer. The signal processing is based on a FFT analysis that provides time resolved shear stress measurements and associated statistics.

The sensor is an optical MEMS-based velocity gradient sensor with body dimensions of 6 mm diameter and 30 mm length. The Micro-S sensor has to be placed flush to the wall with an acceptable uncertainty of ± 5 μm. A laser diode of 15 mW and 659 nm propagates through a fiber optic cable to the probe's head, where a diverging fringe pattern is formed. The diverging interference fringes originate at the surface and extend directly into the flow, as illustrated in Figure 1. Typical dimensions of the measurement volume are 30 μm x 30 μm x 15 μm. The working distance from the wall is 105 μ for air flows and the diverging ratio is 0.066. This technique can provide wall shear stress measurements in the range from 0.015 to 140 Pa.

The scattered light from the particles passing through the fringes is collected by a window at the surface of the sensor. The measurement volume is defined by the intersection of the transmitter and receiver fields. The seeding particles that cross the measurement volume create frequency modulated bursts, similar to LDA characteristic signals, except that the Doppler frequency is now proportional to the velocity gradient at the immediate vicinity of the wall. Considering the asymptotic structure of the classical boundary layer, the velocity distribution along the viscous sublayer in known to be linear. As a consequence, once measurements are performed inside this thin region, the velocity gradient at the wall can be calculated straightforwardly from just one point of measured velocity, as long as its distance from the wall is accurately known. This simple concept summarizes the principle of operation of the Micro-S sensor.
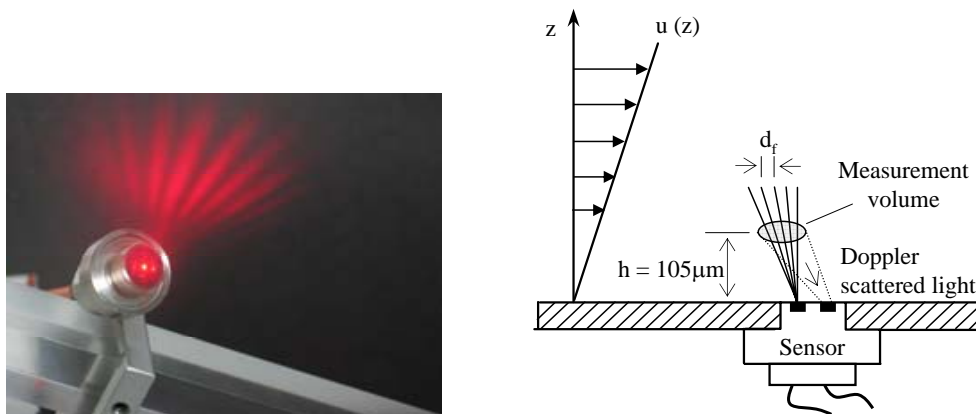
Figure 1. Optical laser-based optical microsensor for shear stress measurements: a) illustration of the probe, b) schematic diagram of the principles of operation.

In analogy to Laser-Doppler anemometry, the measured velocity is linearly dependent on the distance between the fringes, d_f, and on the Doppler frequency f_D, i.e. $u = d_f f_D$. Given the diverging character of the interference fringe pattern, the distance between the fringes is a function of the diverging rate, k, and the distance of the measurement volume from the wall, h, so that $d_f = kh$. From the definition the wall shear stress ($\tau_w = \mu \partial U/\partial z$) we have $\tau_w = \mu d_f f_D/h$, which leads to the direct linear relation between the wall shear stress and the Doppler frequency, i.e. $\tau_w = \mu k f_D$.

The major assets of this technique is that it is non-intrusive, does not require calibration, has a linear response and can be used in any flow problem as long as a viscous sublayer can be identified.

3. EXPERIMENTS

The experiments were carried out in the low-turbulence wind tunnel of the Laboratory of Turbulence Mechanics (PEM/COPPE/UFRJ). The tunnel is an open circuit tunnel with a test section of dimensions 300 mm x 300 mm x 8.000 mm. The roughness elements were fitted into the first four meters. The remaining four meters were fitted with an acrylic surface. A general view of the wind tunnel is shown in Fig. 2.

The rough surface was a transversely grooved surface constructed with rectangular aluminum bars of 6.35 by 4.76 mm

Figure 2. General view of wind tunnel.

rectangular cross section.

Measurements were performed for values of the free-stream velocity of 8 m/s; the free stream-level of turbulence was about 0.2%. Mean velocity and turbulence statistic data were obtained with a two-channel laser Doppler anemometer (LDA) and a two-dimensional particle image velocimeter.

The two-component Dantec laser-Doppler anemometry system used an Ar-ion tube laser and was operated in the forward scatter mode to measure mean and fluctuating velocity fields. A Bragg cell unit was used to introduce a digitally-controlled electronic shift. That was necessary to resolve the direction of the flow field and give correct measurements of near-zero mean velocities. The light beams were made to pass through a series of conditioning optical elements to achieve a small measurement volume and to improve the optical alignment. Front lenses with 500 mm focus length were mounted on the probe to accurately position the measurement volume on the centerline of the channel. Before being collected by the photomultipliers, the scattered light was made to pass through interference filters of 514.5 nm and 488 nm, so that only the green and blue lights were received on each photomultiplier, respectively. Table 1 lists the main characteristics of the laser-Doppler system used. The signals from the photomultipliers were band-pass filtered and processed by a burst spectrum analyzer operating in a single measurement per burst mode. A series of LDA biases were avoided by adjusting the strictest parameters on the data processor. The level validation and the signal to noise ratio were 8 and 5 respectively. For simultaneous measurements of longitudinal and vertical velocities, a coincidence window of 5,000 μs was used. For the statistics at each point, 20,000 samples were considered.

Table 1. Main characteristics of the laser-Doppler system.

Wavelength	514.5 nm (green) 488nm (blue)
Half-angle between beams	1.604^o
Fringe spacing	9.191 μm (green) 8.718 μm (blue)
Beam spacing	28 mm
Beam diameter	2.2 mm
Dimensions of the measurement volume	
Major axis	5.31 mm (green) 5.04 mm (blue)
Minor axis	149.0 μm (green) 141.0 μm (blue)

Typical uncertainties associated with the mean velocity data – U, W – are below 0.2% of the free stream velocity, u_δ. In regions of reverse flow, the uncertainties increase to about 0.3% of the free stream velocity. Regarding the Reynolds stress components – $\overline{u'u'}$, $\overline{w'w'}$, $\overline{u'w'}$ – uncertainties were estimated to be 2.3%, 1.8% and 4.2% of the square of the friction velocity of the undisturbed flow, respectively. In regions of reverse flow, 3.8%, 3.5% and 6.9% are typical values.

The PIV measurements were performed with a two-dimensional Dantec system. The light source was furnished by a double pulsed Nd:YAG laser that produced short duration (10 ns) high energy (120 mJ) pulses of green light (532 nm). The collimated laser beam was transmitted through a cylindrical (15 mm) and a spherical (500 mm) lens to generate a 1 mm thick lightsheet. The reflected light was recorded at 5 Hz by a CCD camera with 1280 x 1024 pixels and 12-bit resolution. The cameras were fitted with a Nikkor 105 mm f/2.8D lenses. The water was seeded with silver-coated glass particles, 10 μm in size. Image calibration was made by taking pictures of a reference target specially designed for the

present purpose.

For all the measurements, the velocity vectors computational conditions were fixed. Adaptive correlation (DaVis 7.1 Software) has been processed on 32 x 32 pixels-size final interrogation spots, with 50% overlap, which gives a 64 x 64 vectors grid. The pixel resolution is 6.45 x 6.45 μm. Particle image treatment consists in using subpixel cell shifting and deformation, allowing bias and random error reduction. A widely accepted estimation of the absolute displacement error using these algorithms is 0.05 pixels. Different thresholds including signal-to-noise ratio and velocity vector magnitude were used as post-processing steps. Residual spurious vectors have been detected using a comparison with the local median of eight neighbour vectors for each grid points. No further filtering has been applied to the velocity fields in order to keep the whole measurement information.

In the present work, seeding was provided by two different types of flow tracers – a fog generator and a Laskin nozzle – and a variety of injection points have been tested. Both flow generators were filled with the same aqueous solution of dialcohol-glycerol mixture. The typical diameter of particles furnished by the fog generator is about 1 μm. The major limitations of fog generators are the intermittent discharge of particles, the high density of the particle flow and the eventual contamination of the surrounding environment by the fog. Droplets produced by the atomizer (Laskin nozzle) vary in size between the range of 0.5 μm to 5.0 μm, with the particle diameter being a function of the pressure of the compressed air feeding line and the working fluid. For the present work, a 5 bar pressure input provided particles of approximately 3 μm in size. Under these conditions, the Laskin nozzle provided a homogeneous and continuous flow of tracer particles, solving the major problems observed with the use of the fog generator.

For both the LDA and PIV techniques the Laskin nozzle provided the best results, assuring a continuously seeded flow with particles that are able to flow field fluctuations but yet scatter enough ligth to provide a good signal to noise ratio. The investigation for the most appropriate injection position showed that conecting the tracer particles directly to the inlet of the fan furnished the most appropriate homogenous distribution of the seeds in flow field rather then injecting the tracer particles immediately downstream the contraction of the wind tunnel or directly in the test section itself.

4. Results

4.1 Mean flow and turbulence statistics

The general flow pattern that is formed in the first two cavities before the smooth surface is reached is shown in Fig. 3 as given by the PIV measurements. Two large regions of recirculating flow are identified, with the formation of stable vortices. Shedding from the protuberances into the flow is significant. In this case, the external flow after passing over the top of a roughness element penetrates deeply into the cavity. In fact, major disturbances are limited to a distance above the crest of the roughness elements of the order of their height, K. These flow features are typical of a 'K'-type surface. A distinct feature of a 'K' type roughness is the absence of a stagnation streamline on the leading face of the cavity. The flow rather is observed to divide around a streamline near the front of the crest. The absence of separated flow on the leading edge of the crest and the presence of trapped stagnant fluid on the trailing side on the cavity are also characteristic of 'K' type surfaces.
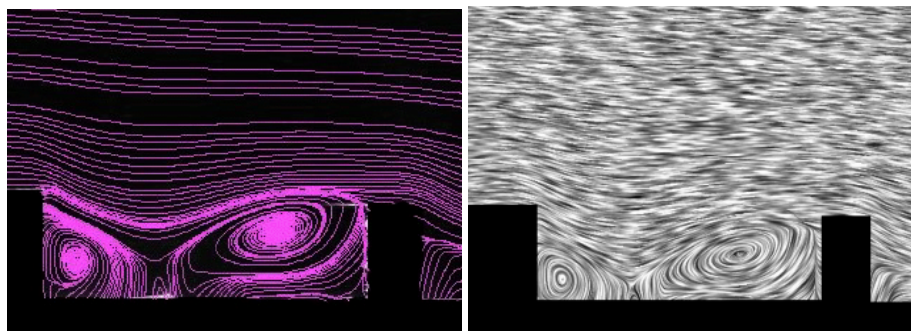
Figure 3. Flow streaklines and streamlines between roughness elements. Flow is from right to left.

The zero-plane displacement, d, was estimated through the procedures of Perry and Joubert (1963) and of Perry et al. (1969). These procedures are very rigorous so that the data resulting from them must be seen as very reliable.

In the Perry and Joubert (1963) and Perry et al. (1969) methods, arbitrary values of d are added to the wall distance measured from the bottom of the roughness elements and a straight line is fitted to the log-law region. The value of d that furnishes the best discriminated logarithmic region is then considered to be the correct value for the zero-plane displacement.

Thus, to determine the zero-plane displacement, the velocity profiles were plotted in semi-log graphs in dimensional coordinates. Next, the normal distance from the wall was incremented by 0.1 mm and a straight line fit was applied

to the resulting points. The best fit was chosen by searching for the maximum coefficient of determination, R-squared. Other statistical parameters were also observed, the residual sum of squares and the residual mean square. Normally, a coefficient of determination superior to 0.99 was obtained.

The velocity gradient method is illustrated in Fig. 4. The plotted velocity profile corresponds to position $x = -77$ mm. The R_{sq} (maximum coefficient of determination, R-squared) values obtained for the various tentatives are also shown. The existence of a well defined maximum value is clear. A quick inspection of Fig. 4b shows that the appropriate value of d is about 3 mm.
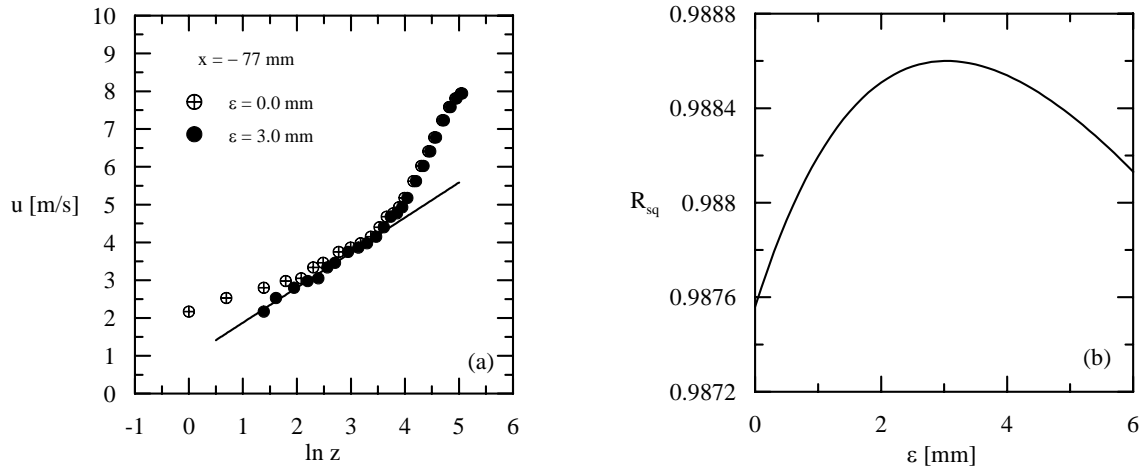
Figure 4. Velocity profile over the rough surface.

Measured velocity profiles for different positions on the smooth surface are shown in Fig. 5. Figure 5a shows clearly that on reaching the smooth wall the flow suddenly accelerates, before the boundary layer starts to readjusts to the new surface conditions.

The distributions of $\sqrt{\overline{u'^2}}$ in Fig. 5b show regions with a very distinct constant behaviour. The level of these nearly constant regions decreases consistently with downstream distance. In the near wall region, $\sqrt{\overline{u'^2}}$ quickly approaches the typical values for flows over smooth walls. The outer part of the boundary layer, on the other hand, persists with its upstream values.

The behaviour of the skewness and flatness factors confirm the expected trends. In turbulent flows, important structural information can be extracted from the higher-order moments. The skewness and flatness factors for the radial velocity fluctuations are defined by

$$S_u = \overline{u'^3}/\left(\overline{u'^2}\right)^{3/2}, \tag{3}$$

$$F_u = \overline{u'^4}/\left(\overline{u'^2}\right)^{2}. \tag{4}$$

Data with a Gaussian distribution satisfy $S_u = 0$ and $F_u = 3$.

At all measuring positions, S_u is negative throughout most of the boundary layer (Fig. 5c). Only very near the wall intense positive fluctuations are recorded ($S_u \approx 0.5$). Flow regions where S_u is positive are associated with acceleration-dominated velocity fluctuations resulting from the arrival of external high-speed fluid (sweep events). Profiles for the flatness (Fig. 5d) show very high values near the wall and in the outer layer, where turbulence is highly intermittent.

4.2 Skin-friction

The MicroS sensor was calibrated against a Preston tube in a wind tunnel.

The values of u_* obtained through the velocity gradient method (Perry and Joubert (1963)) and the MicroS sensor are shown in Fig. 6 for the rough-to-smooth transition region. The calibration curve for the microS sensor is also presented.

The results for the microS sensor are consistently higher than the values obtained through the velocity gradient method. Antonia and Luxton (1972) had previously reported the same conclusion, but with reference measurements provided by a Preston tube. In fact, Antonia and Luxton (1972) write that "none of the standard smooth-wall methods of obtaining skin-friction from mean velocity measurements is reliable for some distance downstream of the roughness change". Their final recommendation is that skin-friction coefficient measurements should be carried out with a floating element balance.
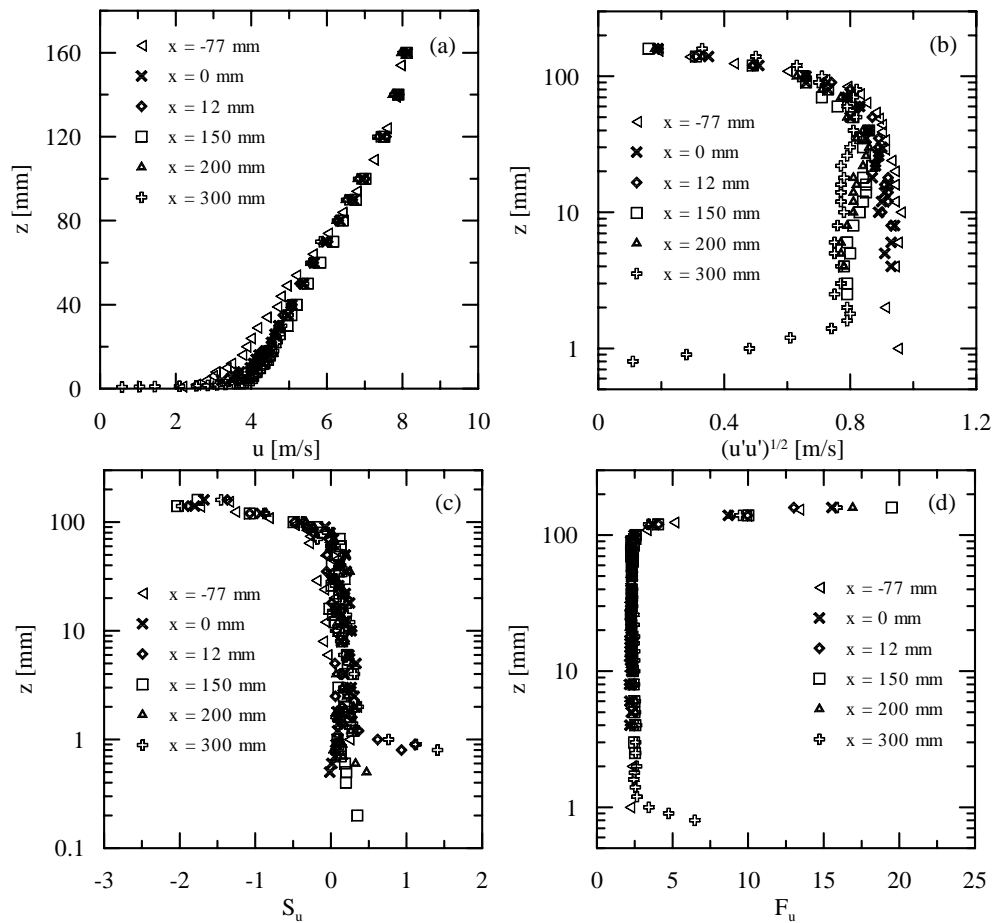
Figure 5. Velocity profiles and turbulence statistics over the smooth wall.

The trend shown in Fig. 6 is the same inferred by Antonia and Luxton (1972). Since there is no cause to doubt the MicroS sensor in the rough-to-smooth transition region, the present results can be considered reference results.

In fact, we have just shown that the gradient of the log-law velocity profile cannot be used to determine u_*.

5. Final Remarks

The calculated values of d and of u_* were obtained through the method of Perry and Joubert (1963) and through the microS sensor. In the first method, by systematically adding an arbitrary value to the distance from the top of the roughness elements, a least square procedure was built to furnish the best discriminated straight line fit. The second method uses the universal calibration curves of Head and Rechenberg (1962) and of Patel (1965).

Determining the wall shear stress has always been a difficult problem that has plagued many authors. In transitional, non-equilibrium regimes, we remind the reader that this problem is aggravated manifold. In this work, results for skin friction in the smooth surface case obtained through the microS sensor were shown to be consistent with the expected trend.

Since the main objective of this work has been to assess the usefulness of the derivative method to evaluate the skin-friction, we feel that this task has been successfully accomplished.

6. ACKNOWLEDGEMENTS
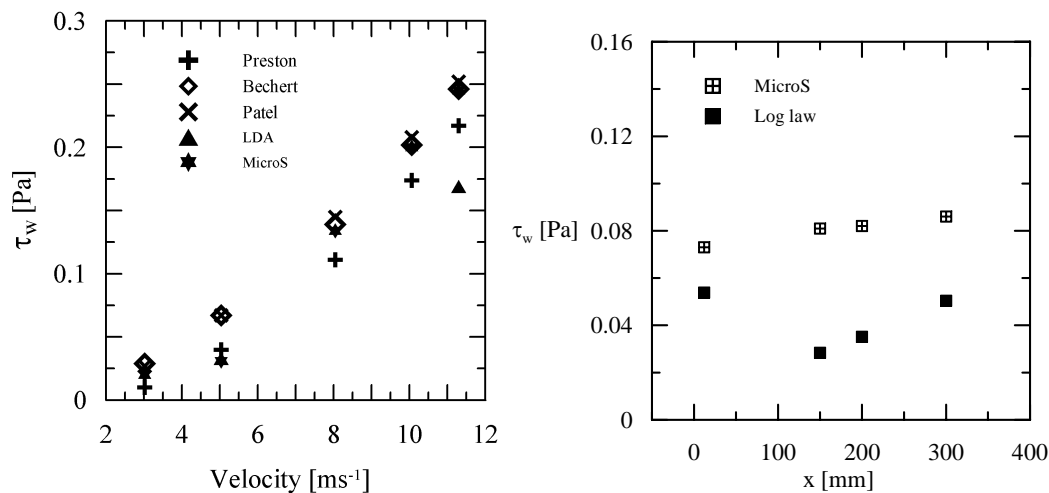
Figure 6. Wall shear stress.

7. REFERENCES

Antonia, R.A. and Luxton, R.E., 1971, The response of a turbulent boundary layer to a step change in surface roughness. Part 1. Smooth to Rough, J. Fluid Mechanics, 48, 721–761.

Antonia, R.A. and Luxton, R.E., 1972,The Response of a Turbulent Boundary Layer to a Step Change in Surface Roughness Part 2. Rough to Smooth, J. Fluid Mechanics, 53, 737–757.

Fourguette, D., Gonzalez, P., Modarress, D., Arik, E., Wilson, D. and Koochesfahani, M., 2004, Optical Measurement of Wall Shear Stress with Emphasis on Flows Near Separation, 24th AIAA Aerodynamic Measurement Technology and Ground Testing Conference, Portland, Oregon.

Head, M.R. and Rechenberg, I., 1962, Preston tube as a means of measuring skin friction, J. Fluid Mechanics, 14, 1–17.

Klebanoff, P.S., 1955. Characterisics of turbulence in a boundary layer with zero pressure gradient. NACA Rep. 1247.

Malhi, Y., 1996, The Behaviour of the Roughness Length for Temperature and Heterogeneous Surfaces, Q. J. R. Meteorol. Soc., 122, 1095–1125.

Patel, V.C., 1965, Calibration of the Preston Tube and Limitations on its Use in Pressure Gradients, J. Fluid Mechanics, 23, 185–208.

Perry, A.E., and Joubert, P.N., 1963, Rough Wall Boundary Layers in Adverse Pressure Gradients, J. Fluid Mechanics, 17, 193–211.

Perry, A.E., Schofield, W.H. and Joubert, P.N., 1969, Rough Wall Turbulent Boundary Layers, J. Fluid Mechanics, 37, 383–413.

Reichardt, H., 1939. Messungen turbulenter Schwankungen. ZAMM 18, 358–361.